Steric Demand and Rate-determining Step for Photoenolization of Di-*ortho*-substituted Acetophenone Derivatives

Anushree Das, Suma S. Thomas, August A. Garofoli, Kevin A. Chavez, Jeanette A. Krause, Cornelia Bohne, & Anna D. Gudmundsdottir

August 2018

Steric Demand and Rate-Determining Step for Photoenolization of Di-*ortho*-Substituted Acetophenone Derivatives

Anushree Das[1], Suma S. Thomas [2], August A. Garofoli [1], Kevin A. Chavez [1], Jeanette A. Krause [1], Cornelia Bohne [2], Anna D. Gudmundsdottir *[1]

[1]. *Department of Chemistry, University of Cincinnati, Cincinnati, OH 45221*, [2] *Department of Chemistry and Centre for Advanced Materials and Related Technologies (CAMTEC), University of Victoria, PO Box 1700 STN CSC, Victoria, BC, Canada, V8W 2Y2*

*Corresponding author e-mail: anna.gudmundsdottir@ uc.edu (Anna D. Gudmundsdottir)

ABSTRACT

Laser flash photolysis of ketone **1** in argon-saturated methanol yields triplet biradical **1BR** (τ = 63 ns) that intersystem crosses to form photoenols *Z*-**1P** (λ_{max} = 350 nm, $\tau \sim 10$ μs) and *E*-**1P** (λ_{max} = 350 nm, $\tau > 6$ ms). The activation barrier for *Z*-**1P** re-forming ketone **1** through a 1,5-H shift was determined as 7.7 ± 0.3 kcal mol^{-1}. In contrast, for ketone **2**, which has a less sterically hindered carbonyl moiety, laser flash photolysis in argon-saturated methanol revealed the formation of biradical **2BR** (λ_{max} = 330 nm, $\tau \sim 303$ ns) that intersystem crosses to form photoenol *E*-**2P** (λ_{max} = 350 nm, $\tau > 42$ μs), but photoenol *Z*-**2P** was not detected. However, in more viscous basic H-bond acceptor (BHA) solvents, such as hexamethylphosphoramide, triplet **2BR** intersystem crosses to form both *Z*-**2P** (λ_{max} = 370 nm, $\tau \sim 1.5$ μs) and *E*-**2P**. Thus, laser flash photolysis of **2** in methanol reveals that that intersystem crossing from **2BR** to form *Z*-**2P** is slower than the 1,5-H shift of Z-**2P**, whereas in viscous BHA solvents the 1,5-H shift becomes slower than the intersystem crossing from **2BR** to **Z-2P**. Density functional theory and coupled cluster calculations were performed to support the reaction mechanisms for photoenolization of ketones **1** and **2**.

INTRODUCTION

Photoenolization is a light-initiated keto–enol tautomerization process, and the resulting photoenols are high-energy ground-state intermediates that are highly reactive (1, 2). Efficient photoenol reactivity has been captured in applications such as synthesizing complex natural products and pharmaceutical drugs, and initiating release from photoremovable protecting groups (3-14). The mechanism of photoenolization, which has been determined using transient spectroscopy, can be outlined as follows: Upon excitation *ortho*-substituted arylketones form the singlet excited state of the ketone chromophore, which undergoes efficient intersystem crossing to form its triplet configuration (<Scheme 1)(15-19). The triplet ketone decays by intramolecular H-atom abstraction to form a triplet 1,4-biradical. Intersystem crossing of the biradical results in the formation of both *Z*- and *E*-photoenols. Generally, *E*-photoenols are long-lived intermediates that can re-form the starting material via a relatively slow solvent-mediated proton transfer, and they are long lived enough to undergo electrocyclic ring closure or be trapped in bimolecular reactions. In contrast, *Z*-photoenols are short-lived intermediates that regenerate the starting material through efficient intramolecular 1,5-H shifts. It should be noted that *ortho*-substituted arylketones that do not undergo efficient intersystem crossing can undergo photoenolization from their singlet ketone to form *Z*-photoenols. Because the lifetimes of *Z*-photoenols are generally on the order of a few nanoseconds, they are too short lived to undergo electrocyclic ring closure or be trapped in bimolecular reactions. Thus, the formation of *Z*-photoenols causes reactions that capture *E*-photoenols in synthetical applications to be less effective, but does not affect reaction selectivity. Thus, a better understanding of the reketonization of *Z*-photoenols has the potential to lead to more efficient use of *E*-photoenols in various applications.

<Scheme 1>

In this study, we compared the photoenolization process for ketones **1** and **2** (<Scheme 2) to determine how photoenolization is affected by substituents. Ketone **1** has two bulky isopropyl groups, whereas ketone **2** has two *ortho* methyl groups. We investigated how the steric demand of the *ortho* substituents affects the 1,5-H shifts in *Z*-photoenols *Z*-**1P** and *Z*-**2P** to re-form the corresponding starting materials, as well as the rate of intersystem crossing of triplet 1,4-biradicals **1BR** and **2BR** to form photoenols *Z*-**1P** and *Z*-**2P**, respectively.

<Scheme 2>

MATERIALS AND METHODS

Laser flash photolysis

Transient UV-Vis spectra and corresponding kinetic traces were acquired using an excimer laser (308 nm, 17 ns) (20). The stock solutions of ketones **1** and **2** were prepared in spectroscopic-grade solvents, such as methanol, acetonitrile, hexamethylphosphoramide (HMPA) and dimethyl sulfoxide (DMSO), so that the absorbance was between 0.2 and 0.8 at 308 nm. Typically, ~1.5 mL of stock solution was placed in a quartz cuvette (10 mm × 10 mm cross-section and 48 mm length). As required, the solution was then purged with argon or oxygen for 5 min. The reaction rates were obtained by fitting an average of 3–8 kinetic traces.

Arrhenius plots. The laser flash photolysis system (YAG laser, 266 nm, 10 ns) has been described in detail elsewhere (21). Methanol solutions of ketones **1** and **2** were prepared in spectroscopic-grade methanol so that the absorbance was ~0.5 at 266 nm. All solutions were purged with N_2 gas before the decays were recorded. The decay rate constants were collected

between 313.15 and 253.15 K for **1** and 313.15 to 233.15 K for **2**. For **1** in methanol, the laser flash photolysis experiment presented some uncertainty as to the baseline. Decays measured with and without the collection of a baseline yielded similar lifetimes. The data obtained from both these experiments were fit simultaneously to yield the parameters reported for the analysis of Arrhenius plots. The kinetic traces obtained from the 266 nm and 308 nm laser irradiation gave similar results.

Calculations

All geometries were optimized using density functional theory (DFT) calculations in Gaussian09 at the B3LYP level of theory with the 6-31+G(d) basis set (22-24), M062X (25), and coupled cluster (26, 27). Time-dependent density functional theory (TD-DFT) calculations were performed to locate the energies of the excited singlet and triplet states of the optimized ground states (28-32). Analysis of the second derivative of the energy with respect to the internal coordinates confirmed that all transition states had one imaginary vibrational frequency. The intrinsic reaction coordinate (IRC) was calculated to verify that the located transition states corresponded to the respective reactant and products (33, 34).

Phosphorescence

Phosphorescence spectra of ketones **1** and **2** were obtained in frozen ethanol matrices at 77 K using a spectrophotometer that has been described in the literature (35).

Synthesis of starting materials

Ketone **2** was purchased from Sigma-Aldrich. Ketone **1** was synthesized as described below.

Ketone **1** was obtained using a procedure similar to that reported by Murphy and Prager (36). 1,3,5-Triisopropylbenzene (1.0 mg, 4.8 mmol) was mixed with acetic anhydride (50 mg, 4.9

mmol) in 10 mL of dichloromethane. After cooling the mixture to 0 °C, $AlCl_3$ (1.3 g, 10 mmol) was added in four portions. The mixture was gradually warmed to room temperature while stirring, and then refluxed for 4 h. Three cubes of ice (~30 mL) were added to the cooled reaction mixture. Once the ice melted, 20 drops of 1 M HCl was added, and the resulting mixture was extracted three times with dichloromethane (20 mL). The organic layer was washed with brine and dried over anhydrous $MgSO_4$,followed by solvent removal under vacuum. The residue was purified by column chromatography using a silica column eluted with a mixture of ethyl acetate and *n*-hexane (20:80, v/v), and ketone **1** was obtained after crystallization from diethyl ether (300 mg, 1.2 mmol, 25% yield). The obtained NMR spectrum was consistent with the reported one in the literature (37).

^{1}H NMR ($CDCl_3$, 400 MHz): δ 7.0 (s, 2H), 2.94–2.83 (m, 1H), 2.77–2.67 (m, 2H), 2.49 (s, 3H), 1.25–1.23 (m, 18H) ppm.

Product studies

A solution of ketone **2** in isopropanol (15 mL, 0.2 mmol, 0.01 M) in a Pyrex round-bottom flask was purged with argon for 20 min, and a rubber cap was fitted to the flask and sealed with parafilm. The resulting solution was irradiated with stirring for ~38 h using a medium-pressure mercury arc lamp. Cyclobutanol **5** was formed in 92% yield.

^{1}H NMR (400 MHz, $CDCl_3$): δ 7.03 (s, 2H), 3.31–3.27 (d, J = 16 Hz, 1H), 3.16–3.12 (d, J = 16 Hz, 1H), 2.29 (s, 3H), 1.69 (s, 3H), 1.30 (s, 9H) ppm. ^{13}C NMR (75 MHz, $CDCl_3$): δ 152.8, 145.9, 140.5, 131.5, 125.5, 118.0, 78.2, 48.1, 35.1, 31.7, 24.8, 16.8 ppm.

RESULTS

Laser flash photolysis in solution

We performed laser flash photolysis (excimer laser, λ = 308 nm, 17 ns) (20) experiments to detect and measure the lifetimes of the 1,4-biradicals and *Z*-photoenols formed by intramolecular H-atom abstraction in ketones **1** and **2**. Laser flash photolysis of ketone **1** in argon-saturated methanol showed broad transient absorption between 310 and 390 nm (<Figure 1A). This absorption was not quenched in oxygen-saturated methanol and thus, it is assigned to photoenols *Z*-**1P** and *E*-**1P**. This assignment is further supported by comparison to the TD-DFT calculated spectra (Figure 1b), which show major electronic transitions at 382 nm (f = 0.1453) and 371 nm (f = 0.1665) for *Z*-**1P** and *E*-**1P**, respectively. Analysis of the kinetics at 350 nm revealed that the transient is formed with a rate constant of 1.58×10^7 s^{-1} (τ = 63 ns, Figure 2a) on a shorter timescale, whereas on a longer timescale the decay can be fitted as a mono-exponential function to yield a rate constant of 1×10^5 s^{-1} ($\tau \sim 10$ μs, Figure 2b). The decay rate constant was not affected by oxygen, which further supports the assignment of the transient absorption to photoenol *Z*-**1P**. On the shorter timescale, the absorption did not decay fully. The small amount of residual absorption decayed on a millisecond timescale and hence, it is assigned to photoenol *E*-**1P**, which has a lifetime of >6 ms. Furthermore, the rate of forming the transient at 350 nm increased in oxygen-saturated methanol to 1.91×10^7 s^{-1} (τ = 52 ns), which indicates that the precursor of *Z*-**1P** decays faster in oxygen-saturated methanol. Thus, the precursor of *Z*-**1P** and *E*-**1P**, triplet 1,4-biradical **1BR**, has a lifetime of ~63 ns in argon-saturated methanol and ~52 ns in oxygen-saturated methanol.

<Figure 1>

<Figure 2>

Laser flash photolysis of ketone **2** in argon-saturated methanol produced a transient spectrum with broad absorption between ~330 and 420 nm (Figure 3a). The two major bands, located at 330 and 350 nm, each exhibited a different kinetic profile. TD-DFT calculations showed that the major electronic transitions for **2BR** are at 413 nm (f = 0.0292), 354 nm (f = 0.0312), and 327 nm (f = 0.0353 nm, Figure 3b), which correlate well with the transient absorbance with λ_{max} at 330 nm. Kinetic analysis of the decay at 330 nm showed that biradical **2BR** decays with a rate constant of 3.4×10^6 s^{-1} (τ = 303 ns) in argon-saturated methanol. In comparison, the transient absorption with λ_{max} at 390 nm can be attributed to either photoenol *Z*-**2P** or *E*-**2P**, or both, as TD-DFT calculations revealed that their major electronic transitions are at 403 nm (f = 0.1189) and 385 nm (f = 0.1359, Figure 3b) for *Z*-**2P** and *E*-**2P**, respectively. Kinetic analysis of the decays at 370 and 390 nm on shorter timescales showed a mono-exponential decay attributed to **2BR**. In contrast, on longer timescales, the decay rate constant was determined to be slower than 2.4×10^4 s^{-1} (τ >42 μs), which is assigned to *E*-**2P**. No transient absorption was observed that can be assigned to Z-**2P** in methanol. Hence, we theorize that biradical **2BR** must be longer lived than *Z*-**2P**; which explains why the only photoenol observed is *E*-**2P**. This notion that the shorter decay rate constant is due to **2BR** and not *Z*-**2P** is further supported by the analysis of the decay in air- and oxygen-saturated methanol. The decay rate constant of **2BR** increased to 1.03×10^7 s^{-1} (τ ~ 97 ns) and 2.5×10^7 s^{-1} (τ ~ 40 ns) in air- and oxygen-saturated methanol, respectively (Figure 3c).

On the contrary, in viscous BHA- solvents, such as DMSO and HMPA, laser flash photolysis of ketone **2** allowed direct observation of both photoenols *Z*-**2P** and *E*-**2P**. Laser flash photolysis of ketone **2** in DMSO and HMPA resulted in transient spectra with λ_{max} at 390 nm (Figure 4a). Kinetic analysis at shorter timescales yielded decay rate constants of 3.8×10^6 and

7.8×10^5 (~300 ns and ~1.5 μs, Figure 4b) for *Z*-**2P** in DMSO and HMPA, respectively. On longer timescales, *E*-**2P** was also detected, decaying on the millisecond timescale. The rate constants for forming *Z*-**2P** and *E*-**2P** were 1.69×10^7 s^{-1} (τ = 52 ns) in argon-saturated HMPA and 2.17×10^7 s^{-1} (τ = 46 ns) in oxygen-saturated HMPA, which are attributed to the decay rate of **2BR**. Thus, viscous BHA solvents have the ability to reduce the rate of the 1,5-H shift in *Z*-**2P**, making this process slower than intersystem crossing, and thus, *Z*-**2P** can be detected directly. For laser flash photolysis data summary see Table S3.

<Figure 3>

<Figure 4>

The formation of *E*-**2P** was further supported by quenching studies in the presence of NaN_3,(38) which assists its reketonization to ketone **2**. Kinetic analysis revealed that the lifetime of *E*-**2P** gradually decreases with the addition of NaN_3 (Figure 5), confirming the formation of *E*-**2P** and its reketonization to **2** can be increased by base in the solvent.

<Figure 5>

Arrhenius plot

Using the Arrhenius equation, $\ln(k_d) = -E_a/RT + \ln(A)$, the decay rate constants of *Z*-**1P** and **2BR**, measured as a function of temperature, were used to determine the activation barriers for the 1,5-H shift in *Z*-**1P** and for **2BR** to twist and intersystem cross to form *Z*-**2P**. The decay rate constant (k_d) of *Z*-**1P** in nitrogen-saturated methanol was monitored at 350 nm. From the slope of the Arrhenius plot (Figure 6), we obtained a transition state barrier of 7.7. ± 0.3 kcal mol^{-1}.

Similarly, the decay rate constant of **2BR** in nitrogen-saturated methanol was monitored at 330 nm as a function of temperature. From the slope of the Arrhenius plot (Figure 6), we obtained a transition state barrier of 4.7 ± 0.1 kcal mol^{-1}, which reflects the barrier for **2BR** to achieve the correct conformation to intersystem cross to photoenols *E*-**2P** and *Z*-**2P**.

<Figure 6>

These results demonstrate that in nitrogen-saturated methanol, the transition state barrier for the 1,5-H shift in *Z*-**1P** is significantly larger than the barrier for intersystem crossing in **1BR**, whereas the 1,5-H shift in *Z*-**2P** must has a smaller transition state barrier than the barrier for intersystem crossing of **2BR**.

Product studies

Photolysis of ketones **1** yields the corresponding cyclobutanol **4**, as reported in previous product studies (39), owing to electrocyclic ring closure of *E*-**1P** (Scheme 3). Similarly, photolysis of ketone **2** in argon-saturated isopropanol forms cyclobutanol **5** via electrocyclic ring closure on *E*-**2P** (Scheme 3).

<Scheme 3>

Calculations

To compare and explain the relative stabilities of the *Z*-enols obtained from ketones **1** and **2**, we performed calculations in Gaussian09 at the B3LYP, M062X, and CBS-QB3 levels of theory using the 6-31+G(d) basis set (22-27). For B3LYP calculations, DFT was used to optimize the

ground states (S_0) of ketones **1** and **2** and their respective triplet excited states, biradicals, and photoenols.

The optimized geometry of the ground state (S_0) of **1** reveals that the carbonyl group is orthogonal to the benzene ring plane owing to steric hindrance created by the two bulky *ortho* isopropyl groups (Figure 7). This configuration leads to a torsional angle of 88° between the C=O and the phenyl ring, revealing that the ketone and phenyl are not conjugated with each other. The optimized geometry is in agreement with the X-ray structure of ketone **1**,(40) which has a torsional angle of 80° between the C=O and the phenyl ring, highlighting the out-of-plane geometry of the carbonyl group. TD-DFT calculations on the optimized S_0 of **1** located its first and second triplet excited states (T_{1K} and T_{2K} of **1**) at 83 and 84 kcal mol^{-1} above S_0 of **1**. These values are considerably higher than the reported energy of the triplet ketone of acetophenone (74 kcal mol^{-1})(41), but more similar to the energies of the triplet ketones of aliphatic ketones such as acetone (79 kcal mol^{-1}) (42), as the C=O chromophore is not conjugated to the phenyl ring.

In comparison, the optimized structure of T_{1K} of **1** is located 72 kcal mol^{-1} above its S_0, which is considerably lower than the energy obtained from the TD-DFT calculations. The torsional angle between the C=O and the phenyl ring is 66° in the optimized structure of T_{1K} of **1**, demonstrating that the C=O and the phenyl group are also not fully conjugated in the T_{1K} of **1**. The C=O bond length in the optimized structure of T_{1K} of **1** is 1.33 Å and the carbon–carbon bonds in the phenyl ring have lengths between 1.39 and 1.43 Å, which suggest a (n,π*) configuration. This configuration is confirmed by spin-density calculations (Scheme 4), which show that the unpaired spin is mainly located on the carbonyl carbon and oxygen atoms.

<Scheme 4>

The optimized structure of **1BR** is located 62 kcal mol^{-1} above the S_0 of **1**, and spin-density calculations show that the unpaired electron density is mainly localized on the *ortho*-carbon and the ketyl carbon atoms, indicating that the radical has a localized 1,4-biradical character. The OH–C–C–CH_2 and $(CH_3)_2$C–C–C–C(OH)(CH_3) torsional angles in **1BR** are 42° and 10°, respectively, and thus **1BR** is less sterically congested than S_0 and T_K of **1**.

<Figure 7>

The optimized structures of *Z*-**1P** and *E*-**1P** are located 38 and 40 kcal mol^{-1}, respectively, above the S_0 of **1**. *Z*-**1P** and *E*-**1P** are twisted $(CH_3)_2$C=C–C=C(OH)(CH_3) torsional angles of 56° and 55°, respectively) owing to the steric demand of the isopropyl group. Photoenols *E*-**1P** and *Z*-**1P** are more twisted than their precursor **1BR**.

Figure 8 displays the calculated stationary points on the energy surface of ketone **1** to form photoenols *E*-**1P** and *Z*-**1P** on the triplet surface. The calculated transition state for hydrogen atom abstraction to form **1BR** is located less than 1 kcal mol^{-1} above T_{1K} of **1**, which is consistent with the spectroscopic observation that intramolecular H-atom abstraction is efficient in **1**.

<Figure 8>

In the optimized structure of ketone **2**, the carbonyl group is not fully conjugated with the phenyl ring owing to presence of two *ortho* methyl substituents (Figure 7). The dihedral angle between the C=O and the phenyl ring is only 51° in S_0 of **2**, confirming that the carbonyl moiety is not fully conjugated with the phenyl ring. However, because the steric demand of the two *ortho* methyl groups in ketone **2** is less than that of the isopropyl groups in ketone **1**, the extent of conjugation between the carbonyl group and the phenyl ring is greater in ketone **2**. The

X-ray structure of ketone **2** also demonstrates that the carbonyl group is not conjugated with the phenyl ring, as the torsional angle between these groups is 80°(43). However, the optimized minimal energy structure of ketone **2** is different from the structure adopted in the crystal lattice, presumably because the best packing arrangement of ketone **2** is achieved with a conformer rather than the minimal energy structure.

TD-DFT calculations estimate that T_{1K} of **2** is located 75 kcal mol^{-1} above its S_0. In comparison, the optimized structure of T_{1K} of **2** is located 70 kcal mol^{-1} above its ground state (Figure 8). Further, the optimized structure of T_{1K} of **2** possesses a torsional angle of only 47° between the C=O and the phenyl ring, and spin-density calculations support that T_{1K} of **2** has a (n,π^*) configuration (Scheme 4).

The optimized structure of **2BR** is located 63 kcal mol^{-1} above S_0 of **2**, and the spin density is mainly localized on the *ortho* and C–OH carbon atoms, with a small contribution on the phenyl ring. As the OH–C–C–CH_2 torsional angle is 48°, the extent of twisting in **2BR** and T_K of **2** is similar. The optimized structures of photoenols *Z*-**2P** and *E*-**2P** are located 40 and 38 kcal mol^{-1}, respectively, above S_0 of **2**. The dienyl moieties are twisted ~40° from planar in both *Z*-**2P** and *E*-**2P**.

The transition state for γ-H atom abstraction by T_{1K} of **2** to form 1,4-biradical **2BR** is located 7 kcal mol^{-1} above T_{1K} of **2**. The calculations show that the steric demand of the *ortho* isopropyl group is significantly larger than that of the *ortho* methyl groups; therefore, **1**, T_K of **1**, **1BR**, *Z*-**1P**, and *E*-**1P** are less planar than **2**, T_K of **2**, **2BR**, *Z*-**2P**, and *E*-**2P**, respectively.

The calculated transition state barriers for 1,5-H shifts in Z-**1P** and Z-**2P** to re-form ketones **1** and **2**, respectively, using various levels of theory are shown in Table 1, along with

the measured barriers obtained from the Arrhenius plots. It should be noted that the energies were calculated with respect to the *Z*-enol conformers, in which the O–H bond points towards the *ortho* methylene. The transition state energies obtained from the B3LYP calculations are not corrected for the zero-point energy, whereas those obtained from the CBS-QB3 calculations are corrected for the zero-point energy. The CBS-QB3 and B3LYP calculated transition state barriers for the 1,5-H shift in *Z*-**1P** correspond well to the experimental value, whereas M062X over estimates it. In comparison, the calculated transition state barrier for the 1,5-H shift in *Z*-**2P** to re-form ketone **2** is smaller than that for Z-**1P** re-form ketone **1**, with B3LYP yielding the smallest barrier and M062X the largest. The measured barrier for intersystem crossing (4.8 kcal mol^{-1}) is similar, within experimental error, to the calculated barrier for the 1,5-H shift.

<Table 1>

In addition, we calculated the transition state barrier for photoenols *E*-**1P** and *E*-**2P** to undergo electrocyclic ring closure to form products **4** and **5**, respectively. These transition states were located 19 and 20 kcal mol^{-1} above photoenols *E*-**1P** and *E*-**2P**, respectively. Thus, the *ortho* substituents do not strongly affect the electrocyclic ring closure reactions of *E*-**1P** and *E*-**2P** (44, 45).

Phosphorescence

The phosphorescence of ketones **1** and **2** was investigated in frozen ethanol glass at 77 K. The phosphorescence spectra of ketones **1** and **2** show vibrational bands characteristic of triplet ketones with (n,π*) configurations, indicating that T_{1K} of **1** and **2** have (n,π*) configurations. However, the vibrational bands are not as well resolved as those for acetophenone derivatives

without *ortho* substituents (Figure 9). Thus, we assigned the [0,0] emission band to the onset of the emission for each ketone to calculate the energies of T_{1K} of **1** and **2** (<Table 2).

<Table 2>

<Figure 9>

We compared the energies of T_{1K} of **1** and **2** obtained from the phosphorescence spectra to those obtained from calculations using B3LYP and M062X hybrid functions. The energies from the TD-DFT calculations are in excellent agreement with the energies obtained from the phosphorescence spectra. In contrast, the energies obtained from the optimized structures of T_K of **1** and **2** using both M062X and B3LYP are somewhat lower than the experimentally obtained values.

DISCUSSION

Ketone **1** undergoes efficient H-atom abstraction on the triplet surface and forms both *Z*- and *E*-photoenols. The measured transition state barrier for *Z*-**1P** to re-form ketone **1** through a 1,5-H shift is 7.7 ± 0.3 kcal mol^{-1}, and this step is slower than intersystem crossing to form Z-**1P**. Because the $CH_3C=C–C=COHCH_3$ torsional angle in photoenol *Z*-**1P** significantly deviates from planarity to accommodate the steric demand of the isopropyl group, *Z*-**1P** must untwist to generate a planar conformer with good orbital alignment for the 1,5-H shift. In contrast, there is less steric congestion around the carbonyl moiety of ketone **2**, and therefore the rate-determining step for its photoenolization is the intersystem crossing of **2BR** to form photoenols **2P**. Photoenol *Z*-**2P**, which is well aligned for undergoing a 1,5-H shift to re-form ketone **2**, reacts faster than it is formed and therefore, it is not observed. The calculated transition state barrier

for the 1,5-H shift in *Z*-**2P** is considerably less than that for *Z*-**1P**. However, the measured barrier for intersystem crossing of **2BR** is on the same order as the calculated transition state barrier for the 1,5-H shift in **2BR**, and therefore, it is possible to influence the rate of photoenolization and re-ketonization, so in viscous BHA solvents the 1,5-H shift of becomes the slowest step.

Haag et al. previously demonstrated that in the photoenolization of *o*-methylacetophenone, intersystem crossing to form photoenols is the slowest step in solvents, such as cyclohexane, methanol, and isopropanol. whereas in more viscous BHA solvents, such as HMPA and DMSO, the 1,5-H shift is sufficiently restricted to become slower than intersystem crossing of the triplet biradical precursor(1). Thus, our results mirror those of Haag and co-workers for the photoenolization of *o*-methylacetophenone. In comparison, we have shown that Z-photoenols from o-methyl substituted valerophenone and butyrophenone ester derivatives re-ketonize slower than their biradical precursors.(18,19) Similarly, 2,5-dimethylphenacyl ester derivatives also form Z-photoenols that are longer-lived than their triplet biradical precursors.(46) Thus, it is not well understood what factors control the intersystem crossing rates of triplet biradicals involved in photoenolization of o-methylacetophenone derivatives.

Interestingly, it has been proposed that the formation of cyclobutanols from *ortho*-substituted arylketones in the solid state do not occur through photoenolization, but rather through direct intersystem crossing of the biradicals to form cyclobutanols (47, 48). This notion was supported by laser flash photolysis of nanocrystals, which revealed that *E*-photoenols are not observed. Because the energies and the structures of biradicals **1BR** and **2BR** are similar to the energies and structures of the calculated transition state barrier for forming cyclobutanols **4** and **5**, respectively, it is possible that in some media, it is favorable to cross over from the triplet surface of the biradical to that of the cyclobutanol through a conical intersection (Figure 10). As

the energy gap between biradicals **1BR** and **2BR** and the calculated transition state barriers for the 1,5-H shifts is larger, it is unlikely that the biradicals can intersystem cross to re-form the corresponding ketones directly, without first forming *Z*-**1P** and *Z*-**2P**.

<Figure 10>

CONCLUSION

In this work, we demonstrated that steric crowding around the carbonyl group in *ortho*-substituted aryl ketones affects the photoenolization process. For photoenol *Z*-**2P**, the transition state barrier for the 1,5-H shift is on the same order as the rotation barrier required for intersystem crossing from its precursor **2BR**. Therefore, the reaction environment controls whether intersystem crossing of **2BR** or the 1,5-H shift of Z-**2P** is the slowest process. In contrast, as photoenol *Z*-**1P** has more steric crowding, the transition state barrier to re-form ketone **1** through the 1,5-H shift is significantly larger than the rate for intersystem crossing from **1BR**.

ACKNOWLEDGEMENTS: We acknowledge funding from NSF (CHE-1464694) and the Ohio Supercomputer Center for supporting this work. AD is grateful for generous support from the Chemistry Department at the University of Cincinnati including a RITE fellowship. Researchers at UVic thank NSERC (RGPIN-121389-2012) for funding and CAMTEC for the use of shared facilities.

REFERENCES

1. Haag, R., J. Wirz and P. J. Wagner (1977) The photoenolization of 2-methylacetophenone and related compounds. *Helv. Chim. Acta* **60,** 2595-2607.
2. Yang, N. C. and C. Rivas (1961) A new photochemical primary process , the photochemical enolization of o-substituted benzophenones. *J. Am. Chem. Soc.* **83,** 2213-2213.
3. Klán, P., T. Š. Solomek, C. G. Bochet, A. l. Blanc, R. Givens, M. Rubina, V. Popik, A. Kostikov and J. Wirz (2013) Photoremovable protecting groups in chemistry and biology: Reaction mechanisms and efficacy. *Chem. Rev.* **113,** 119-191.
4. Klan, P., J. Wirz and A. D. Gudmundsdottir (2012) Photoenolization and its applications. In *In CRC Handbook of Organic Photochemistry & Photobiology, 3rd Edition,* Vol. 1. (Edited by A. Griesbeck, M. Oelgemoller and F. Chetti), pp. 627-652. CRC Press, Boca Raton, FL.
5. Sankaranarayanan, J., S. Muthukrishnan and A. D. Gudmundsdottir (2009) Photoremovable protecting groups based on photoenolization. *Adv. Phys. Org. Chem.* **43,** 39-77.
6. Mayer, G. and A. Heckel (2006) Biologically active molecules with a "light switch". *Angew. Chem., Int. Ed.* **45,** 4900-4921.
7. Herrmann, A. Using photolabile protecting groups for the controlled release of bioactive volatiles. *Photochem. Photobio. Sci.* **11,** 446-459.
8. Dell'Amico, L., A. Vega-Penaloza, S. Cuadros and P. Melchiorre (2016) Enantioselective organocatalytic Diels-Alder trapping of photochemically generated hydroxy-o-quinodimethanes. *Angew. Chem., Int. Ed.* **55,** 3313-3317.
9. Moorthy, J. N., P. Mal, N. Singhal, P. Venkatakrishnan, R. Malik and P. Venugopalan (2004) Highly diastereoselective tandem photoenolization-hetero-diels-alder cycloaddition reactions of o-tolualdehydes in the solid state. *J. Org. Chem.* **69,** 8459-8466.
10. Nicolaou, K. C., D. L. F. Gray and J. Tae (2004) Total synthesis of hamigerans and analogues thereof. Photochemical generation and Diels-Alder trapping of hydroxy-o-quinodimethanes. *J. Am. Chem. Soc.* **126,** 613-627.
11. Nicolaou, K. C. and D. L. F. Gray (2004) Total synthesis of hybocarpone and analogues thereof. A facile dimerization of naphthazarins to pentacyclic systems. *J. Am. Chem. Soc.* **126,** 607-612.
12. Pelliccioli, A. P. and J. Wirz (2002) Photoremovable protecting groups: Reaction mechanisms and applications. *Photochem. Photobio. Sci.* **1,** 441-458.
13. Pika, J., A. Konosonoks, R. M. Robinson, P. N. D. Singh and A. D. Gudmundsdottir (2003) Photoenolization as a means to release alcohols. *J. Org. Chem.* **68,** 1964-1972.
14. Konosonoks, A., P. J. Wright, M.-L. Tsao, J. Pika, K. Novak, S. M. Mandel, J. A. Krause Bauer, C. Bohne and A. D. Gudmundsdóttir (2005) Photoenolization of 2-(2-methyl benzoyl) benzoic acid, methyl ester: Effect of E-photoenol lifetime on the photochemistry. *J. Org. Chem.* **70,** 2763-2770.
15. Pelliccioli, A. P., P. Klán, M. Zabadal and J. Wirz (2001) Photorelease of HCl from o-methylphenacyl chloride proceeds through the Z-xylylenol. *J. Am. Chem. Soc.* **123,** 7931-7932.
16. Guerin, B. and L. J. Johnston (1989) Laser flash photolysis studies of 2,4,6-trialkylphenyl ketones. *Can. J. Chem.* **67,** 473-480.
17. Small, R. D. and J. C. Scaiano (1977) Role of biradical intermediates in the photochemistry of o-methylacetophenone. *J. Am. Chem. Soc.* **99,** 7713-7714.
18. Das, A., E. A. Lao and A. D. Gudmundsdottir (2016) Photoenolization of o-methylvalerophenone ester derivative. *Photochem. Photobio.* **92,** 388-398.

19. Muthukrishnan, S., J. Sankaranarayanan, T. C. S. Pace, A. Konosonoks, M. E. DeMichiei, M. J. Meese, C. Bohne and A. D. Gudmundsdottir (2010) Effect of alkyl substituents on photorelease from butyrophenone derivatives. *J. Org. Chem.* **75,** 1393-1401.
20. Muthukrishnan, S., J. Sankaranarayanan, R. F. Klima, T. C. S. Pace, C. Bohne and A. D. Gudmundsdottir (2009) Intramolecular H-atom abstraction in γ-azido-butyrophenones: Formation of 1,5 ketyl iminyl radicals. *Org. Lett.* **11,** 2345-2348.
21. Liao, Y. and C. Bohne (1996) Alcohol effect on equilibrium constants and dissociation dynamics of xanthone–cyclodextrin complexes. *J. Phys. Chem.* **100,** 734-743.
22. Frisch, M. J., G. W. Trucks, H. B. Schlegel, G. E. Scuseria, M. A. Robb, J. R. Cheeseman, G. Scalmani, V. Barone, B. Mennucci, G. A. Petersson, H. Nakatsuji, M. Caricato, X. Li, H. P. Hratchian, A. F. Izmaylov, J. Bloino, G. Zheng, J. L. Sonnenberg, M. Hada, M. Ehara, K. Toyota, R. Fukuda, J. Hasegawa, M. Ishida, T. Nakajima, Y. Honda, O. Kitao, H. Nakai, T. Vreven, J. A. Montgomery Jr, J. E. Peralta, F. o. Ogliaro, M. J. Bearpark, J. Heyd, E. N. Brothers, K. N. Kudin, V. N. Staroverov, R. Kobayashi, J. Normand, K. Raghavachari, A. P. Rendell, J. C. Burant, S. S. Iyengar, J. Tomasi, M. Cossi, N. Rega, N. J. Millam, M. Klene, J. E. Knox, J. B. Cross, V. Bakken, C. Adamo, J. Jaramillo, R. Gomperts, R. E. Stratmann, O. Yazyev, A. J. Austin, R. Cammi, C. Pomelli, J. W. Ochterski, R. L. Martin, K. Morokuma, V. G. Zakrzewski, G. A. Voth, P. Salvador, J. J. Dannenberg, S. Dapprich, A. D. Daniels, Ã. d. n. Farkas, J. B. Foresman, J. V. Ortiz, J. Cioslowski and D. J. Fox (2009) Gaussian 09. Gaussian, Inc., Wallingford, CT, USA.
23. Becke, A. D. (1993) Density functional thermochemistry. III. The role of exact exchange. *J. Phys. Chem.* **98,** 5648-5652.
24. Lee, C., W. Yang and R. G. Parr (1988) Development of the colle-salvetti correlation-energy formula into a functional of the electron density. *Phys. Rev. B* **37,** 785-789.
25. Zhao, Y. and D. G. Truhlar (2008) The M06 suite of density functionals for main group thermochemistry, thermochemical kinetics, noncovalent interactions, excited states, and transition elements: Two new functionals and systematic testing of four M06-class functionals and 12 other functionals. *Theor. Chem. Acc.* **120,** 215-241.
26. Montgomery, J. A., M. J. Frisch, J. W. Ochterski and G. A. Petersson (2000) A complete basis set model chemistry. VII. Use of the minimum population localization method. *J. Phys. Chem.* **112,** 6532-6542.
27. Montgomery, J. A., M. J. Frisch, J. W. Ochterski and G. A. Petersson (1999) A complete basis set model chemistry. VI. Use of density functional geometries and frequencies. *J. Phys. Chem.* **110,** 2822-2827.
28. Labanowski, J. K. and J. W. Andzelm (1991) Density functional methods in chemistry. (Edited by K. L. Jan and W. A. Jan), pp. 443. Springer-Verlag New York, Inc.
29. Parr, R. G. and Y. Weitao (1989) *Density functional theory in atoms and molecules*. Oxford University Press: Oxford.
30. Stratmann, R. E., G. E. Scuseria and M. J. Frisch (1998) An efficient implementation of time-dependent density-functional theory for the calculation of excitation energies of large molecules. *J. Phys. Chem.* **109,** 8218-8224.
31. Bauernschmitt, R. D. and R. Ahlrichs (1996) Treatment of electronic excitations within the adiabatic approximation of time dependent density functional theory. *Chem. Phys. Lett.* **256,** 454-464.
32. Foresman, J. B., M. Head-Gordon, J. A. Pople and M. J. Frisch (1992) Toward a systematic molecular orbital theory for excited states. *J. Phys. Chem.* **96,** 135-149.

33. Gonzalez, C. and H. B. Schlegel (1990) Reaction path following in mass-weighted internal coordinates. *J. Phys. Chem.* **94,** 5523-5527.
34. Gonzalez, C. and H. B. Schlegel (1989) An improved algorithm for reaction path following. *J. Chem. Phys.* **90,** 2154-2161.
35. Ranaweera, R. A. A. U., T. Scott, Q. Li, S. Rajam, A. Duncan, R. Li, A. Evans, C. Bohne, J. P. Toscano, B. S. Ault and A. D. Gudmundsdottir (2014) Trans–cis isomerization of vinylketones through triplet 1,2-biradicals. *J. Phys. Chem. A* **118,** 10433-10447.
36. Murphy, R. and R. H. Prager (1978) Organoboranes in organic synthesis: Ix. Carbonylation products of organoboranes derived from myrcene. *J. Organom. Chem.* **156,** 133-147.
37. Hog Daniel, T. and M. Oestreich (2009) $B(C_6F_5)_3$-catalyzed reduction of ketones and imines using silicon-stereogenic silanes: Stereoinduction by single-point binding. *Eur. J. Org. Chem.* **2009,** 5047-5056.
38. Scaiano, J. C., V. Wintgens and J. C. Netto-Ferreira (1992) Scavenging of photoenols by acids and bases. *Tetrahedron Lett.* **33,** 5905-5908.
39. Kitaura, Y. and T. Matsuura (1971) Photoinduced reactions—XLVIII: Steric and substituent effects on photoreactions of 2,4,6-trialkylphenyl ketones. *Tetrahedron* **27,** 1597-1606.
40. Blair, A. D., A. D. Hendsbee and J. D. Masuda (2011) 1-(2,4,6-Triisopropylphenyl)ethanone. *Acta Crystallogr. Sect. E* **67,** o2731.
41. Ghoshal, S. K., S. K. Sarkar and G. S. Kastha (1981) Effects of intermolecular hydrogen-bonding on the luminescence properties of acetophenone, characterization of emission states. *Bull. Chem. Soc. Jpn.* **54,** 3556-3561.
42. Borkman, R. F. and D. R. Kearns (1966) Electronic-relaxation processes in acetone. *J. Phys. Chem.* **44,** 945-949.
43. van Koningsveld, H., J. J. Scheele and J. C. Jansen (1987) Structure of 4-tert-butyl-2,6-dimethylacetophenone and comparison with its $FeCl_3$ complex. *Acta Crystallogr. Sect. C* **43,** 294-296.
44. Muthukrishnan, S., T. C. S. Pace, Q. Li, B. Seok, G. de Jong, C. Bohne and A. D. Gudmundsdottir (2011) Comparison of photoenolization and alcohol release from alkyl-substituted benzoyl benzoic esters. *Can. J. Chem.* **89,** 331-338.
45. Li, Q., J. Sankaranarayanan, M. Hawk, V. T. Tran, J. L. Brown and A. D. Gudmundsdottir (2012) The effects of h-bonding and sterics on the photoreactivity of a trimethyl butyrophenone derivative. *Photochem. Photobio. Sci.* **11,** 744-751.
46. Zabadal, M., A. P. Pelliccioli, P. Klán and J. Wirz (2001) 2,5-dimethylphenacyl esters: A photoremovable protecting group for carboxylic acids. *J. Phys. Chem. A* **105,** 10329-10333.
47. Kuzmanich, G., J. Xue, J.-C. Netto-Ferreira, J. C. Scaiano, M. Platz and M. A. Garcia-Garibay (2011) Steady state and transient kinetics in crystalline solids: The photochemistry of nanocrystalline 1,1,3-triphenyl-3-hydroxy-2-indanone. *Chemi. Sci.* **2,** 1497-1501.
48. Ito, Y., H. Takahashi, J.-Y. Hasegawa and N. J. Turro (2009) Photocyclization of 2,4,6-triethylbenzophenones in the solid state. *Tetrahedron* **65,** 677-689.

Table 1. Calculated transition state barriers for 1,5-H shifts in *Z*-photoenols and experimental transition state barriers.

	Calculated transition state barrier for 1,5-H shift (kcal mol^{-1})			Experimentally measured transition state barrier (kcal mol^{-1})	
	B3LYP	M062X	CBS-QB3	1,5-H shift	Intersystem crossing
Z-**1P**	7.60	10.57	8.35	7.7 ± 0.3	
Z-**2P**	4.79	7.22	6.299		4.7 ± 0.1

Table 2. Experimental and calculated energies (kcal mol^{-1}) of T_{1K} of **1** and **2**.

Ketone	Phosphorescence	B3LYP		M062X	
		TD-DFT	Optimization	TD-DFT	Optimization
1	82 (350 nm)	83	72	81	73
2	77 (373 nm)	75	70	77	74

FIGURE CAPTIONS

Figure 1. A) Transient spectra obtained by laser flash photolysis of **1** in argon-saturated methanol. B) TD-DFT calculated spectra of **1BR**, *Z*-**1P**, and *E*-**1P**.

Figure 2. A) Kinetic trace obtained from laser flash photolysis of ketone **1** in argon-saturated methanol at 350 nm. B) Kinetic traces for the decay of *Z*-**1P** in argon- (red) and oxygen-saturated methanol (black) at 350 nm.

Figure 3. Transient spectra obtained by laser flash photolysis of **2** in argon-saturated methanol. B) TD-DFT calculated spectra of **2BR**, *Z*-**2P**, and *E*-**2P**. C) Kinetic trace obtained by laser flash photolysis of ketone **2** in argon- (red) and oxygen-saturated methanol (black) at 350 nm.

Figure 4. A) Transient spectra obtained by laser flash photolysis of **2** in argon-saturated HMPA. B) Kinetic traces obtained at 330 nm in argon- and oxygen-saturated HMPA.

Figure 5. Kinetic traces at 330 nm obtained by laser flash photolysis of **1** in argon-saturated methanol as a function of added of NaN_3 (1 M).

Figure 6. Arrhenius plots of the decay rate constants obtained by laser flash photolysis of ketone **1** at 350 nm and ketone **2** at 330 nm in nitrogen-saturated methanol as a function of temperature.

Figure 7. Optimized structures of **1**, **1BR**, *E*-**1P**, and *Z*-**1P** and **2**, **2BR**, *E*-**2P**, and *Z*-**2P** using B3LYP/6-31+G(d).

Figure 8. Calculated stationary points on the energy surfaces of ketones A) **1** and B) **2**. Energies are in kcal mol^{-1}.

Figure 9. Phosphorescence spectra of ketones A) **1** and B) **2** obtained in ethanol glass at 77 K.

Figure 10. Calculated IRC graphs for the transitions state for forming cyclobutanol **4** from *E*-**1P** (black dots) and ketone **1** from *Z*-**1P** (red dots).

Scheme 1.

Scheme 2.

Scheme 3.

Scheme 4. Calculated spin densities for T_{1K} of **1** and T_{1K} of **2**.

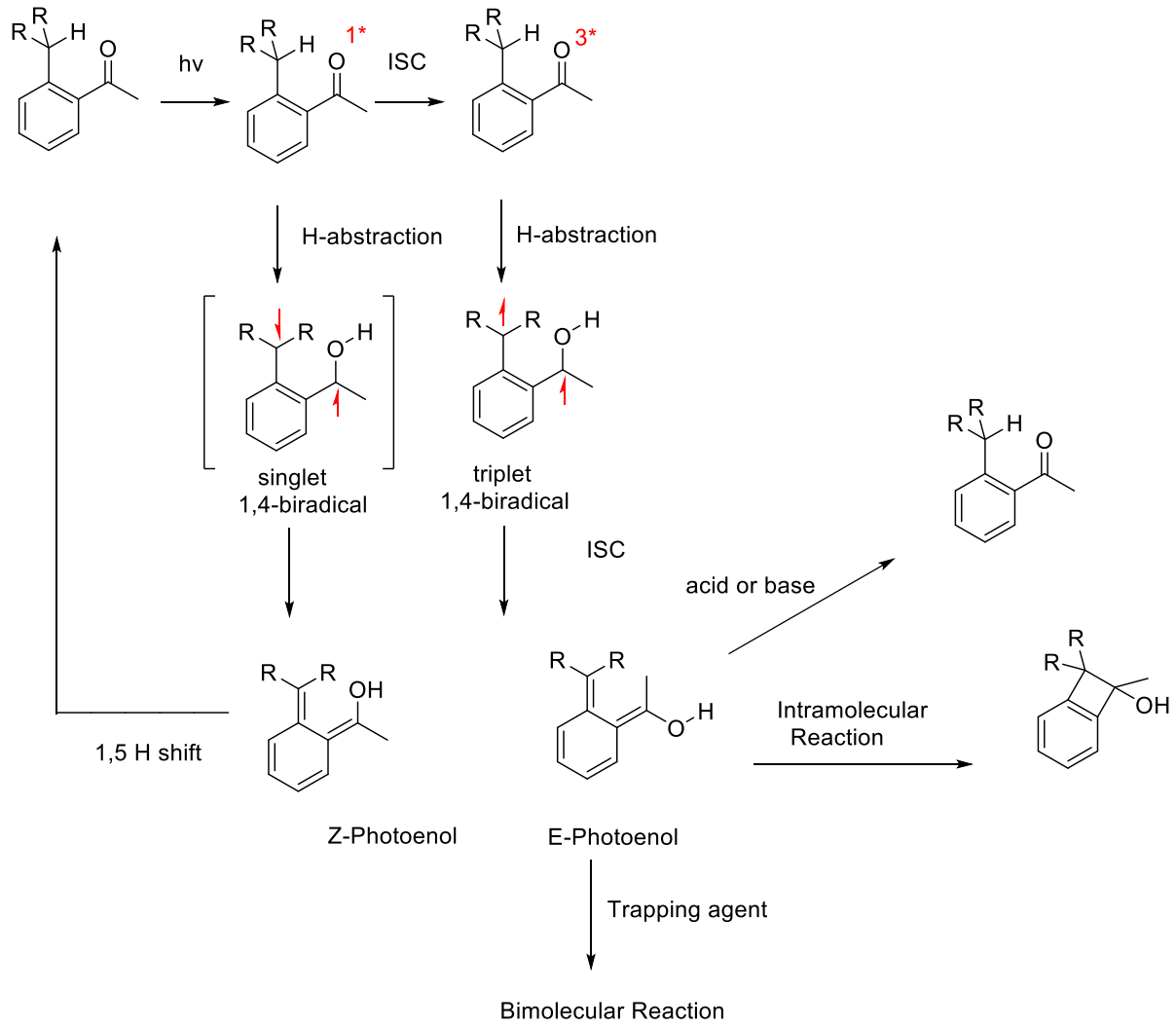

524

525 Scheme 1

526

527

528

529

530

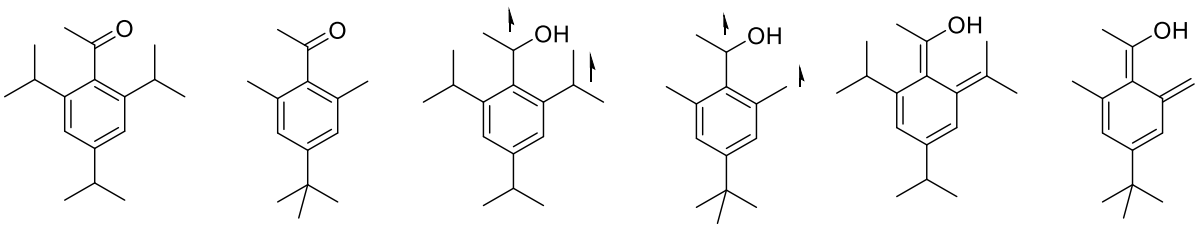

1 **2** **1BR** **2BR** **Z-1P** **Z-2P**

531 Scheme 2

532

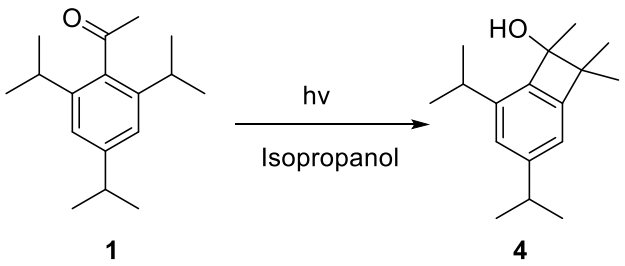

1 **4**

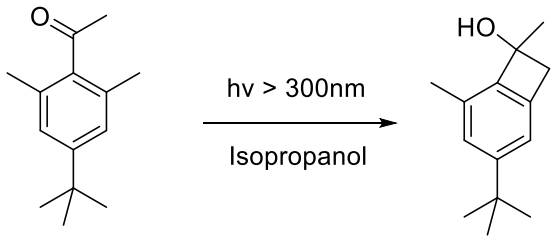

2 **5**

533

534 Scheme 3

535

536

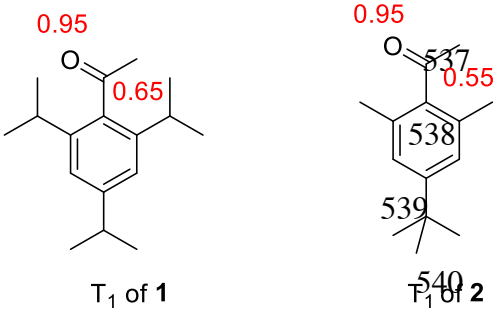

T_1 of **1** T_1 of **2**

541 Scheme 4

542

543 Figure 1

544

A

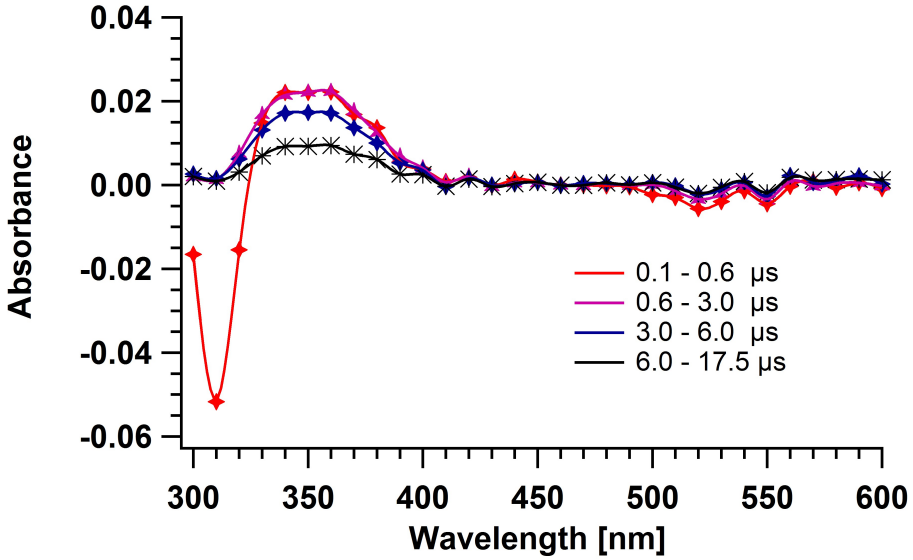

B

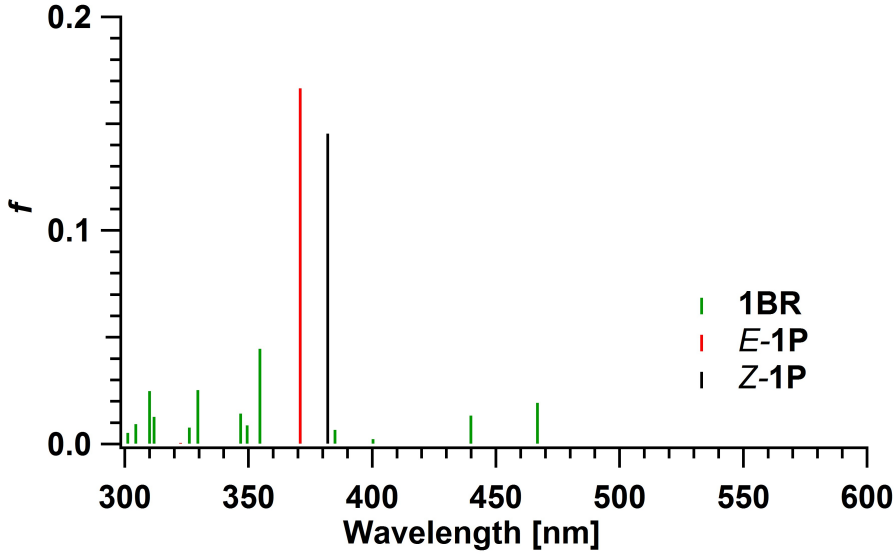

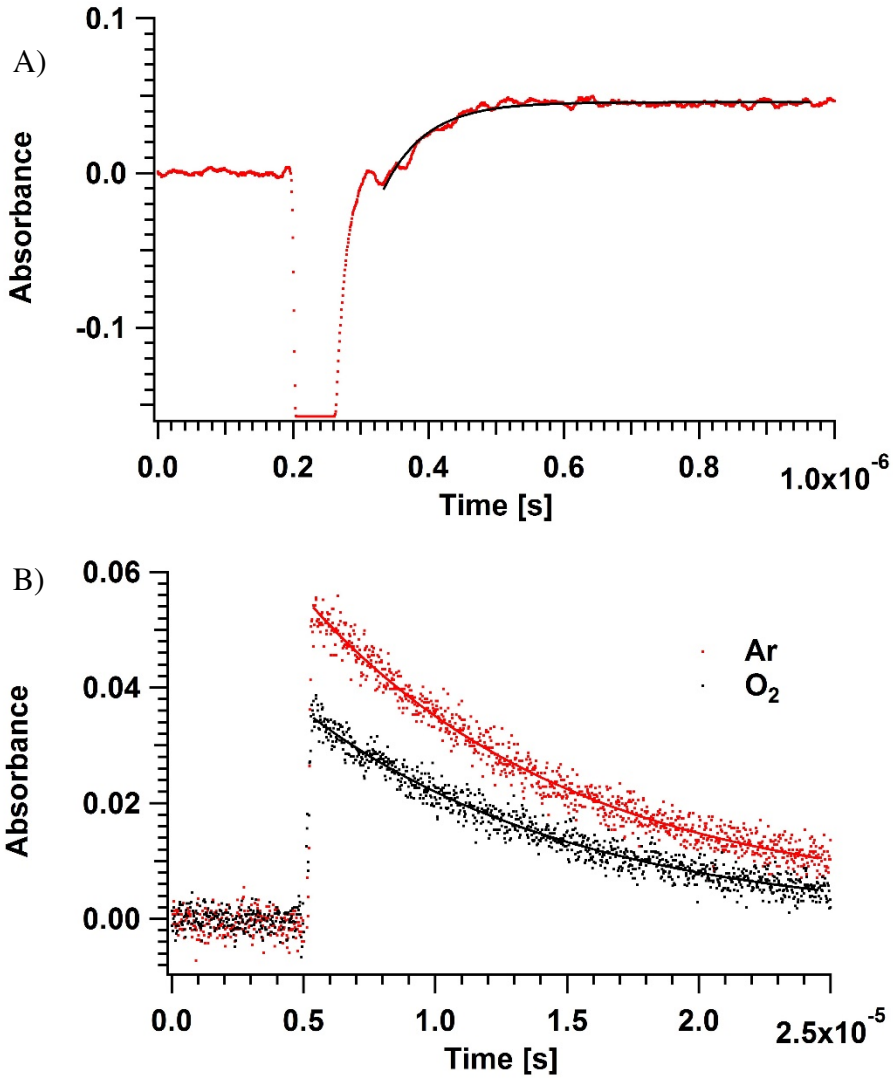

545 Figure 2

546

547

A)

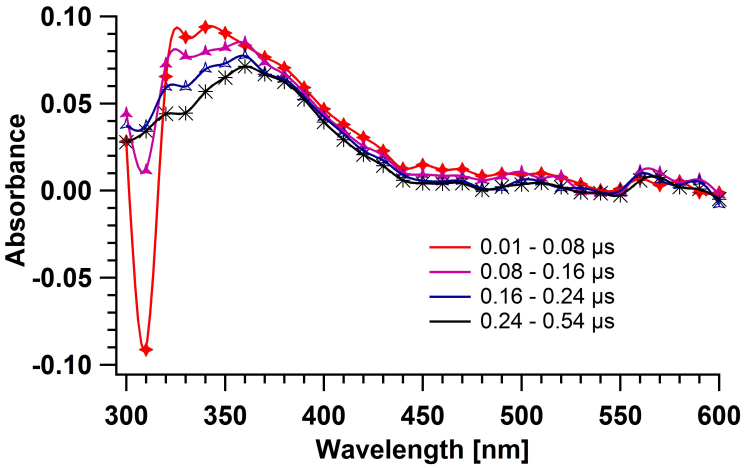

B)

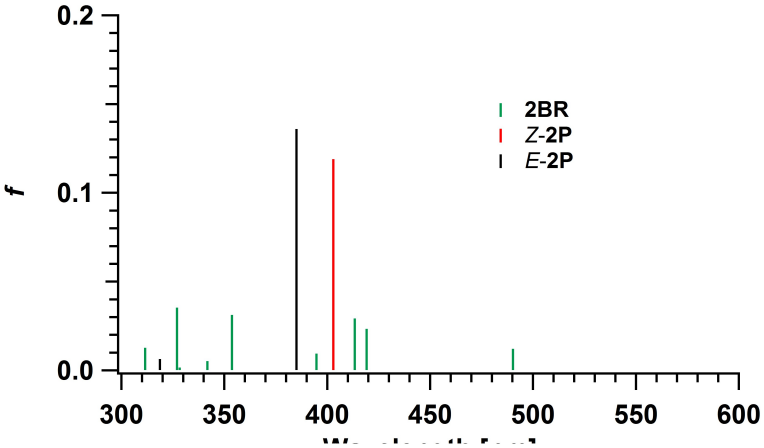

C)

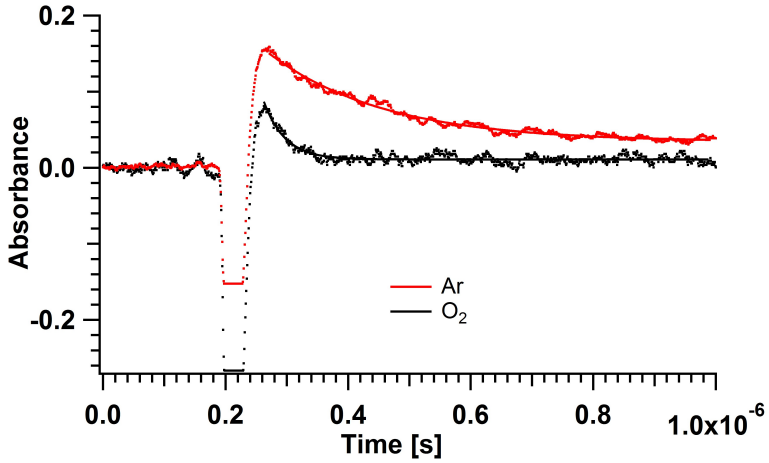

548 Figure 3

549

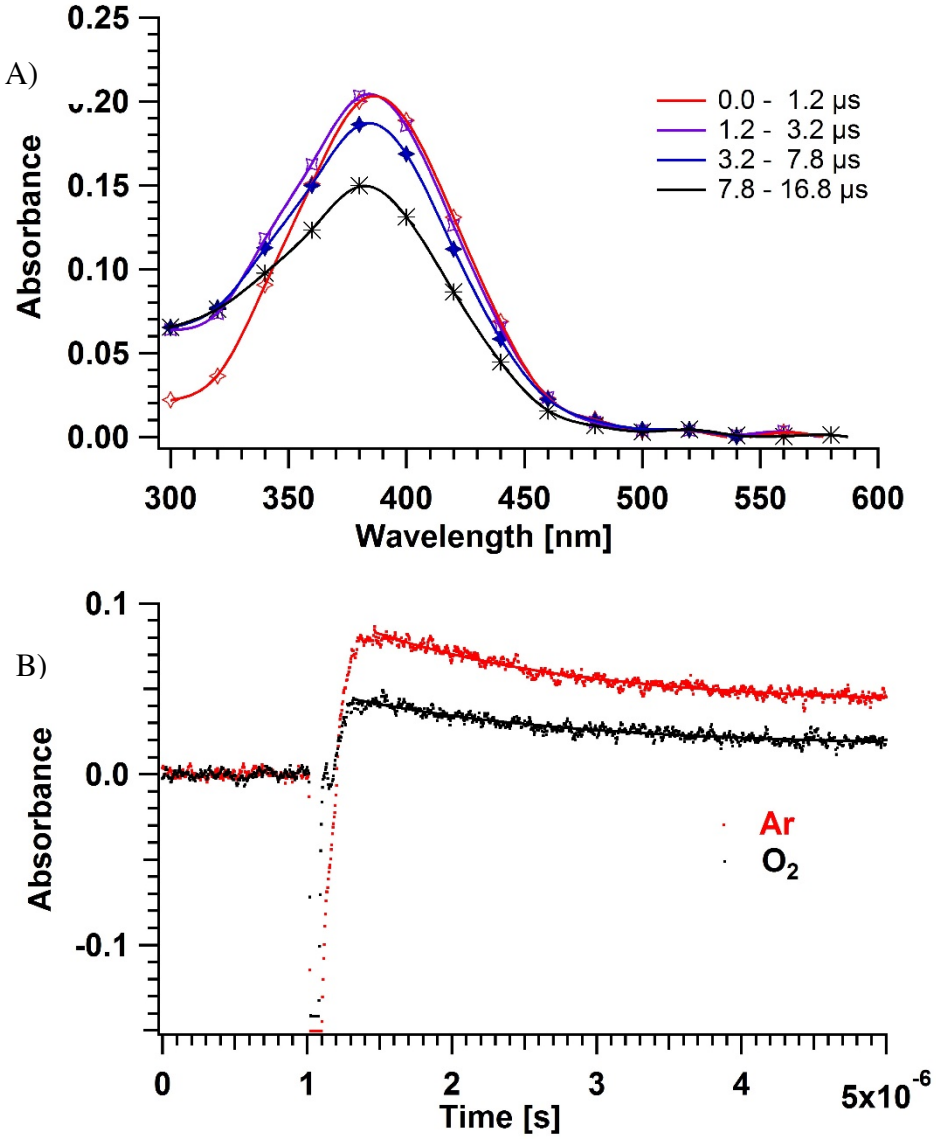

550 Figure 4

551

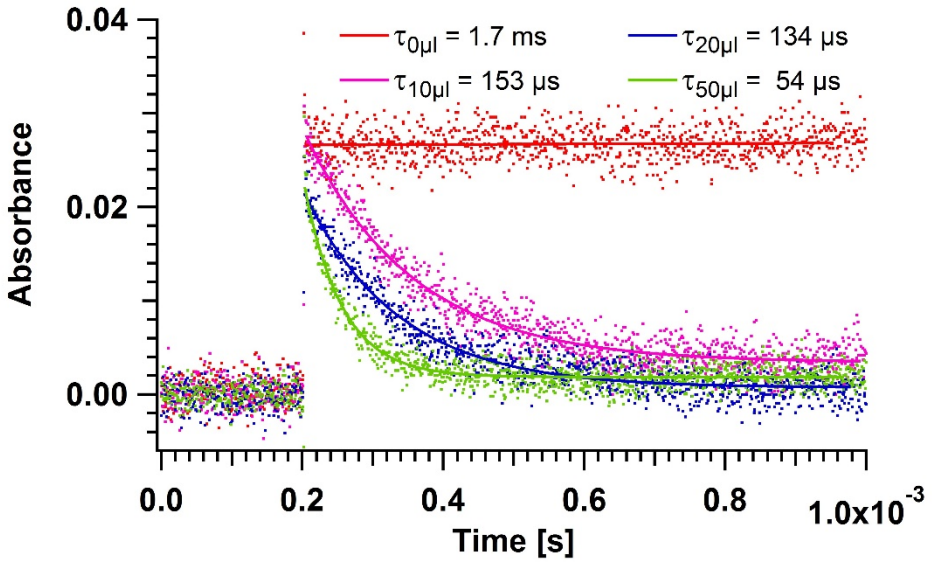

552 Figure 5

553

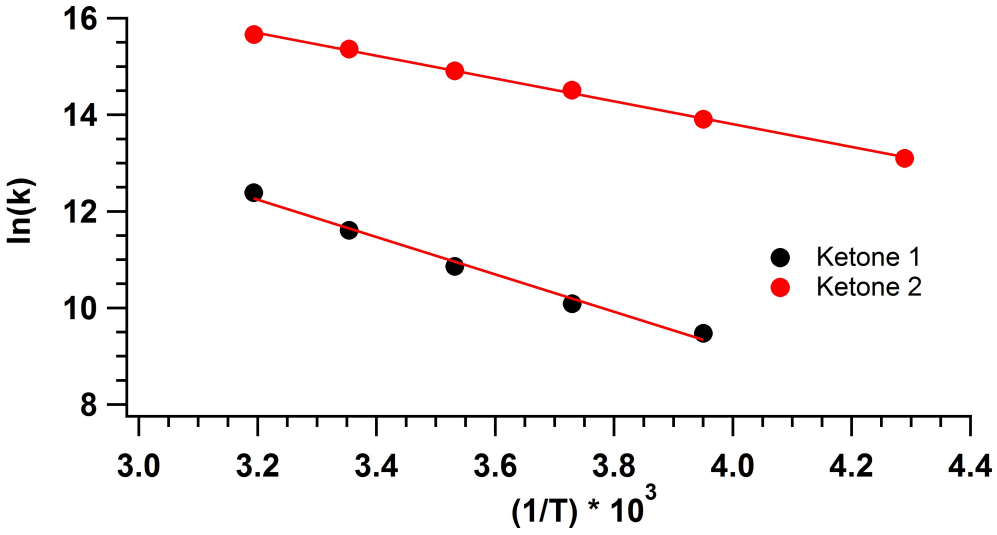

554

555 Figure 6

556

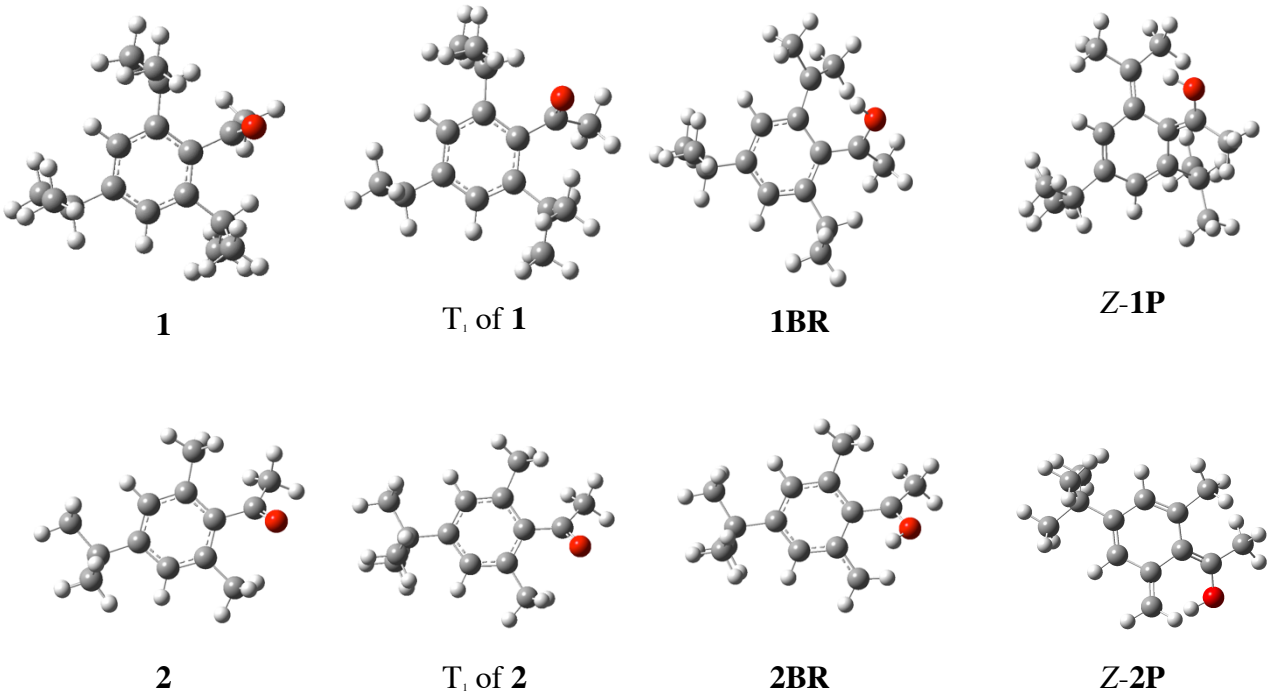

557 Figure 7

558

A)

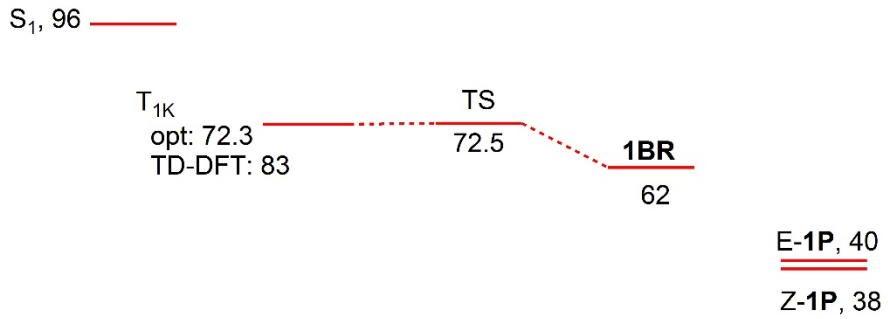

B)

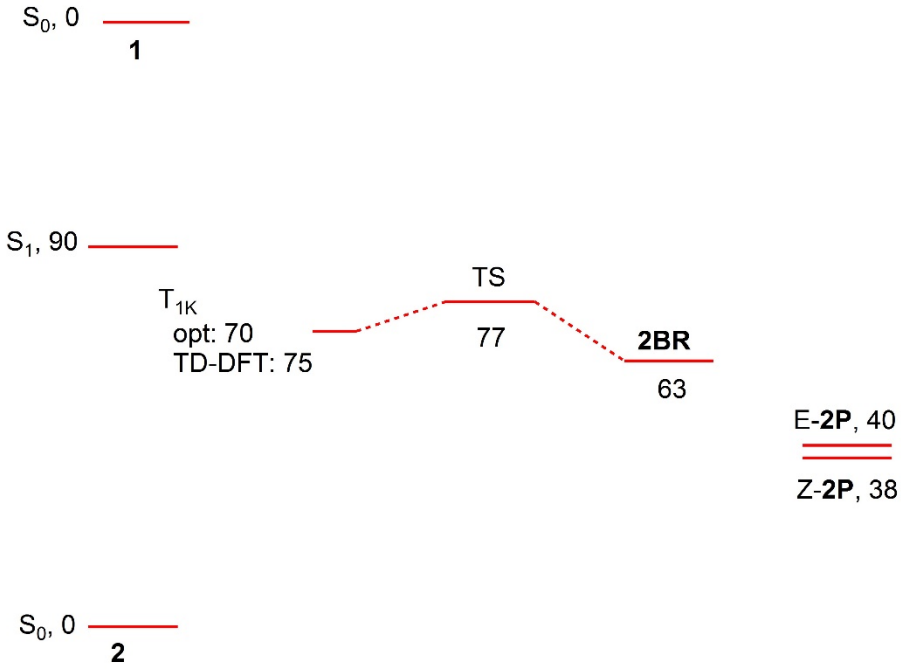

559 Figure 8

560

A)

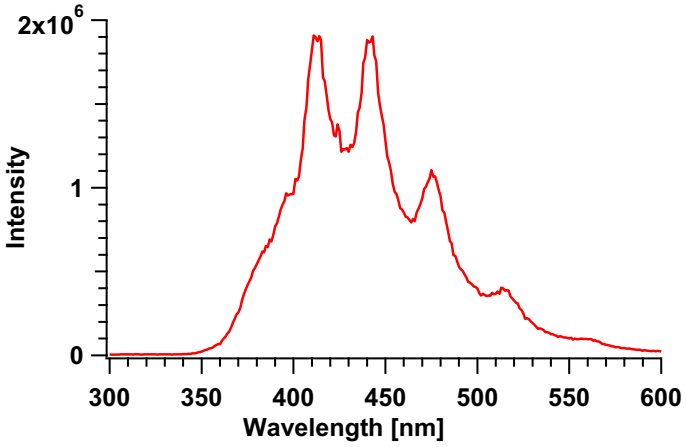

B)

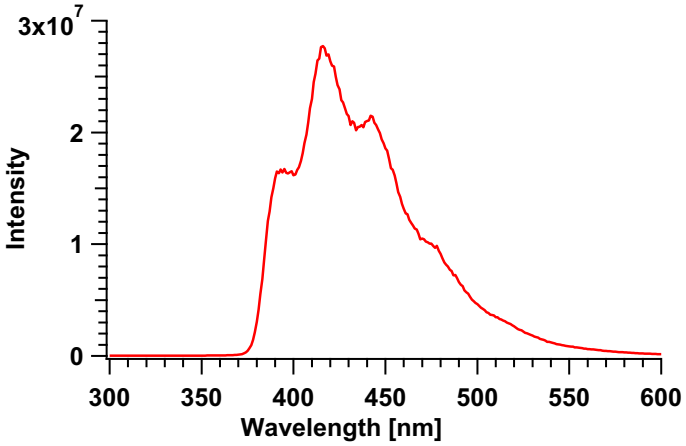

561 Figure 9

562

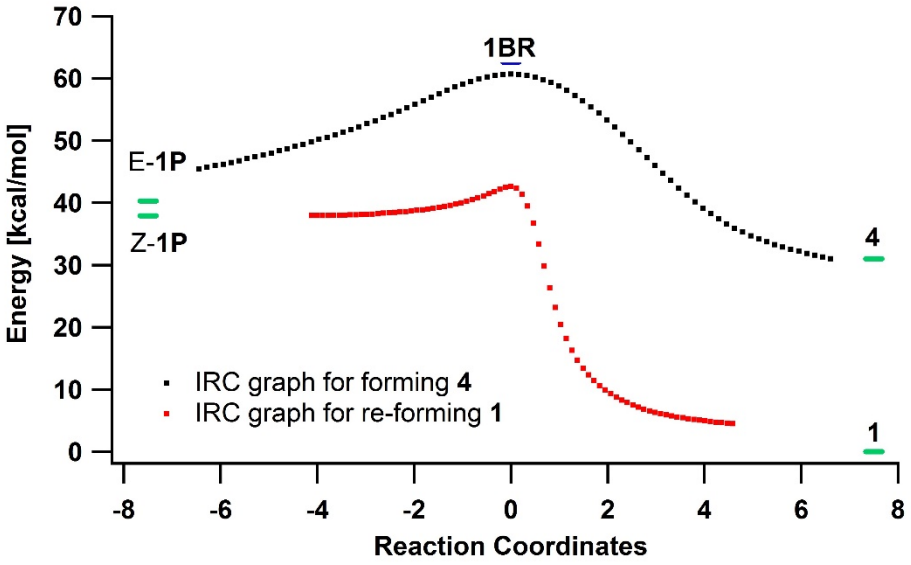

563 Figure 10